

DOI: 10.1002/

Article type: ((Full Paper))

## Stabilizing Li-S Battery Through Multilayer Encapsulation of Sulfur

*Younes Ansari, Sonia Zhang, Bohua Wen, Frank Fan, Yet-Ming Chiang\**

Dr. Y. Ansari, S. Zhang, Dr. B. Wen, Dr. F. Fan, Prof. Y. -M. Chiang

Department of Materials Science and Engineering, Massachusetts Institute of Technology,  
Cambridge, MA 02139, USA

E-mail: [ychiang@mit.edu](mailto:ychiang@mit.edu)

Prof. Y. -M. Chiang

Department of Materials Science and Engineering, Massachusetts Institute of Technology,  
Cambridge, MA 02139, USA

Keywords: lithium sulfur battery, multilayer encapsulation, polypyrrole, manganese oxide, stabilized cathode

**Abstract:** Advancements in portable electronic devices and electric powered transportation has drawn more attention to high energy density batteries, especially lithium-sulfur battery due to the lower cost of sulfur and its high energy density. However, the lithium-sulfur battery is still quite far from commercialization mostly because of incompatibility between all major components of the battery – the cathode, anode and electrolyte. Here we demonstrate a methodology that shows promise in significantly improving battery stability by multilayer encapsulation of sulfur particles, while using

This is the author manuscript accepted for publication and has undergone full peer review but has not been through the copyediting, typesetting, pagination and proofreading process, which may lead to differences between this version and the [Version of Record](#). Please cite this article as [doi: 10.1002/aenm.201802213](https://doi.org/10.1002/aenm.201802213).

This article is protected by copyright. All rights reserved.

conventional electrolytes, which allows a long cycle life and an improved coulombic efficiency battery at low electrolyte feeding. Our multilayer encapsulated sulfur battery demonstrates a coulombic efficiency as high as 98%, when a binder-free electrode is used. We also show that the all-out self-discharge of the cell after 168 hrs can be reduced from 34% in the regular sulfur battery to less than 9% in the battery with the multilayer encapsulated sulfur electrode.

## 1. Introduction

There are more than one billion cars on the road running on fossil fuels and such over-consumption leads to serious environmental issues. Therefore, the development of alternative strategies for energy storage are essential if clean energy technologies that can displace fossil fuels are to be successful. Although the number of electric vehicles (EVs) has increased over the past few years, they cannot yet deliver the same user experience as gasoline powered cars, mainly because of the cost and the lower driving range of these vehicles using the current battery technologies. To resolve such issues, novel ideas for production of cheap, high energy-density, and long cycle life rechargeable batteries are compelling. Among various types of batteries, the lithium-sulfur (Li-S) battery is a promising candidate since it delivers a remarkable theoretical capacity of 1672 mAh g<sup>-1</sup> (S) and a theoretical specific energy up to 2600 Wh kg<sup>-1</sup> compared with the state-of-the-art high voltage cathode batteries with theoretical specific energy of approximately 600 Wh kg<sup>-1</sup>. In addition, elemental sulfur is environmentally friendly, inexpensive and abundant.

The Li-S battery poses some challenges that need to be overcome. One of the major challenges of the Li-S battery is that it generally suffers from the shuttling of soluble polysulfide species (Li<sub>2</sub>S<sub>x</sub>, x=4-

8) during cycling, which results in a low coulombic efficiency and reduces its cycle life, typically to less than 100 cycles. In addition, since sulfur<sup>[1]</sup> and lithium sulfide are electronic insulators, the electronic conductivity of the cathode typically has to be augmented by addition of a significant amount of conductive carbon. To overcome these issues, most efforts have been directed to prevent soluble polysulfides from shuttling, by encapsulation of sulfur with conducting membranes or porous structures<sup>[2-29]</sup>, most recently through designing 3D cathode architectures<sup>[30,31,32,33,34]</sup> or other sulfur hosts<sup>[35,36]</sup> which allow improved stability as well as fast kinetics. Among conductive polymers, polypyrrole has been widely investigated<sup>[20,26,28,37]</sup> owing to its high electronic conductivity, low cost of precursors and ease of synthesis. However, studies of polypyrrole encapsulated sulfur composites have shown no major successes perhaps due to the presence of large pores (~5nm, **Figure S1** in the **supporting information**) in the encapsulating polymer. In addition, encapsulated sulfur nano-composites require dissolution of a certain amount of sulfur by organic solvents to provide a void space in order to accommodate the large volumetric expansion of sulfur upon lithiation.<sup>[26]</sup>

Here, for the first time, we demonstrate a strategy to improve the stability of Li-S battery using a multilayer encapsulation of sulfur nano-particles. To ensure an effective encapsulation of sulfur, the following coating layers are selected. We coat the sulfur nano-particles with MnO<sub>2</sub> particles as the interior shell since it was demonstrated that soluble lithium polysulfide species can be easily oxidized to thiosulfate groups by MnO<sub>2</sub> particles. The thiosulfate groups formed on the surface of the MnO<sub>2</sub> are proposed to anchor long-chain polysulfides by catenating them to form polythionates and therefore catalyze their conversion to insoluble short-chain polysulfides which significantly minimizes the shuttle effect.<sup>[29]</sup> We use polypyrrole as the exterior shell since (a) its porous structure allows electrolyte uptake, (b) its flexible network supports and contains the inner MnO<sub>2</sub> shell during

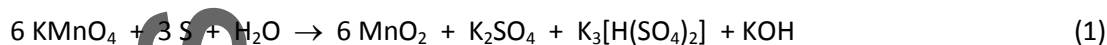
discharging where the volumetric expansion of sulfur occurs, and (c) its remarkable electronic conductivity improves the bulk conductivity of the electrode and provides electronic charge transfer to the sulfur nanoparticles.

We show that our composite sulfur particles can deliver a significant improvement in the battery cycling performance, even with high sulfur loading ( $>2.5 \text{ mg cm}^{-2}$ ). We also demonstrate that through multi-layer encapsulation of sulfur, the capacity decay due to the self-discharge issue can be reduced considerably (less than 9% after 168 hrs of rest), compared with the significant self-discharge fade ( $\sim 30\text{-}40\%$ ) in a typical Li-S battery<sup>[38]</sup>. Our galvanostatic cycling of the nano-composite working electrode in cells with 5.0 mL/g-S and 7.0 mL/g-S shows that lower E/S ratio results in a higher capacity retention, which can be attributed to a change in the pore morphology when the electrode is soaked with an excessive amount of electrolyte. This is in marked contrast with other studies that show consistently inferior cycle life at low E/S ratios.<sup>[39]</sup> It should be noted that electrochemical analysis of as-developed Li-S electrodes of this study have been performed based on the standards suggested by the techno-economic modeling.<sup>[40]</sup> Our engineered electrodes help in achieving Li-S batteries with high sulfur loading as high as  $\sim 3 \text{ mg cm}^{-2}$  and low electrolyte (E) to sulfur (S) ratio of approximately 5 mL/g-S.

## 2. Multi-layer encapsulated sulfur nano-particle (SPPyMnO<sub>2</sub>)

The schematic diagram for the synthesis and morphology of SPPyMnO<sub>2</sub> nano-composites is illustrated in **Figure 1a**. Sulfur nanoparticles were initially formed by reacting sodium thiosulfate (Na<sub>2</sub>S<sub>2</sub>O<sub>3</sub>) with concentrated hydrochloric acid (HCl) in an aqueous solution of polyvinylpyrrolidone.

The sulfur nano-particles were then coated with polypyrrole to form a sulfur/polypyrrole (SPPy) nano-composite through the oxidative polymerization of pyrrole (monomer) in the presence of the iron chloride/methyl orange template (FeCl<sub>3</sub>/MO) at room temperature. The sulfur in the SPPy was then reacted with potassium permanganate (KMnO<sub>4</sub>) at room temperature to form MnO<sub>2</sub> nano-sheets through the following reaction:<sup>[41]</sup>



FeCl<sub>3</sub>/MO is known to be a complex and a reactive template that immediately forms after the addition of methyl orange (MO) to a solution of FeCl<sub>3</sub>. This complex can serve as a morphology guiding agent as well as an oxidant.<sup>[42]</sup> Our synthetic result shows that polypyrrole nucleates on the surface of sulfur particles with the aid of this template. The template has previously shown to assist growth of polypyrrole nanotubes.<sup>[43]</sup> During sulfur encapsulation, the template (FeCl<sub>3</sub>/MO) tends to cover the surface of SPPy nano-spheres (please see the **supporting information, Figure S2a**) and prevent prevalent growth of polypyrrole which results in the formation of large clusters of the polymer and inhomogeneous encapsulation of sulfur nanoparticles. The template may then be simply removed by using a dilute solution of hydrochloric acid and a solution of ammonium persulfate, to leave the segregated spherical SPPy nano-particles behind (**Figure S2b**). We note that in the absence of the template, nonuniform layers of polypyrrole were formed, which led to partial encapsulation of sulfur nanoparticles (**Figure S3**).

An SEM image of the polymer coated sulfur nano-particles (SPPy) is shown in **Figure 1b**. **Figure 1c** shows the SEM image of the SPPy nano-particles which were further treated with  $\text{KMnO}_4$  to form a layer of  $\text{MnO}_2$  in between sulfur nano-particles and the polypyrrole membrane, to yield the SPPy $\text{MnO}_2$  composite. A TEM image of the SPPy $\text{MnO}_2$  nano-particles is shown in **Figure 1d**, which confirms non-aggregating nano-particle formation with an average size of  $\sim 700\text{nm}$ .

It has been previously shown that the result of **equation 1** is a crystalline structure of  $\delta\text{-MnO}_2$ , while the same reaction in the presence of a coating membrane results in the formation of amorphous manganese oxide nano-sheets. The powder X-ray diffraction pattern of the SPPy $\text{MnO}_2$ , shown in **Figure 2a**, reveals that sulfur as the only crystalline phase in the composite. XRD pattern of the bare sulfur nano-particles confirms presence of orthorhombic (Fddd) sulfur nano-particles. The XRD pattern of SPPy composites did not exhibit significant changes except for the presence of a broad peak which is associated with the amorphous nature of polypyrrole. The amorphous structure of polypyrrole is also shown in **Figure 2b** and the inset shows the TEM image of SPPy $\text{MnO}_2$  nano-particles after dissolution of the encapsulated sulfur nano-particles, using toluene as solvent, which further confirms presence of  $\text{MnO}_2$  nano-sheets with distinguishable boundaries and an encapsulating layer of polypyrrole on top of sulfur nano-particles.

The FTIR spectra of polypyrrole and SPPy are shown in **Figure S4**. For both polypyrrole and SPPy the absorption peaks at  $801$  and  $928\text{ cm}^{-1}$  are related to C-H out-of-phase and in-phase bending vibrations, respectively.<sup>[44,45]</sup> The C=C double bond stretching vibrations in the pyrrole ring were observed at  $1560\text{ cm}^{-1}$  and  $1480\text{ cm}^{-1}$ , and the peaks at  $1710\text{ cm}^{-1}$  and  $1300\text{ cm}^{-1}$  are exposed as C=N and C-N bonds, respectively.<sup>[46,47]</sup> For SPPy, the peak at  $475\text{ cm}^{-1}$  corresponds to the vibrational spectrum of orthorhombic sulfur crystals ( $\alpha\text{-S}_8$ )<sup>48</sup>. The FTIR spectrum of the template ( $\text{FeCl}_3/\text{MO}$ ) is

also shown in **Figure S4**. The FTIR spectrum of the template ( $\text{FeCl}_3/\text{MO}$ ) is also shown in **Figure S4**. This spectrum is in agreement with the identified peaks for methyl orange (marked with stars). The peak at  $610\text{ cm}^{-1}$  corresponds to the vibrational frequency of the Fe-O bond. From the FTIR spectrum of the template, it is evident that polypyrrole and SPPy are free of template materials contamination. **Figure S5** shows the result of XPS analysis of the SPPyMnO<sub>2</sub> powder. **Figure S5a**, the Mn 2p spectrum, exhibits two distinct peaks, Mn 2p<sub>3/2</sub> at 640.8 eV and Mn 2p<sub>1/2</sub> at 652.2 eV. The binding energy difference between the Mn 2p<sub>3/2</sub> and Mn 2p<sub>1/2</sub> peaks is about 11.4 eV which is in agreement with the values reported for the Mn<sup>4+</sup> oxidation state.<sup>[49,50]</sup> **Figure S5b** shows the O 1s spectrum of the SPPyMnO<sub>2</sub> sample. The peak at 529.1 eV can be ascribed to (Mn–O–Mn). The presence of Mn (IV), O, C, N, and a small amount of K (< 3%) is confirmed, while possible contaminants Na, Fe and Cl are not detected. The small amount of potassium could be due to the existence of  $\text{K}_x\text{MnO}_{2-5}$  ( $x \sim 0.15$ ) or potassium ions in the composite.<sup>[41]</sup>

The results of the thermogravimetric analysis (TGA) are shown in **Figure 3**. These results were used to determine the amount of active material (sulfur) and calculate the specific capacity values in the SPPy and SPPyMnO<sub>2</sub> composites. The initial weight loss profiles between 30-117 °C are due to the elimination of any residual water and sublimation of sulfur prior to melting. The weight loss associated with polypyrrole decomposition ends at approximately 230°C. The percentage of sulfur in SPPy and SPPyMnO<sub>2</sub> composites is determined to be 84.7 and 82.5 wt%, respectively. **Figure S6** compares the TGA thermograms and the derivative curves between SPPy, SPPyMnO<sub>2</sub>, and neat polypyrrole. The TGA result shows the higher thermal stability of the polypyrrole produced by the

method presented in this paper compared to sulfur that is present in the SPPy and SPPyMnO<sub>2</sub> composites. According to this figure, at 275 °C, while 100% of the sulfur is lost, most of the polypyrrole (> 80%) has remained intact. Therefore, the weight loss below 275 °C corresponds to sulfur rather than polypyrrole.

### 3. Electrochemical performance of SPPy and SPPyMnO<sub>2</sub>

The cycling performance and coulombic efficiency of the cells with bare sulfur, SPPy and SPPyMnO<sub>2</sub> cathode materials at C/5, are compared in **Figure 4a**. The cyclability and coulombic efficiency of SPPyMnO<sub>2</sub> with various amounts of electrolyte at C/5 and C/2 are also compared. This figure suggests a significant improvement in capacity retention of the SPPyMnO<sub>2</sub> electrode compared with SPPy and bare sulfur electrodes, while bare sulfur showed the least capacity retention. At C/2, SPPyMnO<sub>2</sub> maintained its capacity retention at 67% after 500 cycles with 7mlE/g-S of electrolyte and at 74% with 5mlE/g-S. Polypyrrole has been shown to expand up to 20% in contact with liquid electrolyte, due to entrance of the anions into the polymer matrix.<sup>[51,52]</sup> In addition, excess liquid electrolyte has been shown to improve ionic conductivity across the polypyrrole membrane.<sup>[53]</sup> BET measurements of polypyrrole nanospheres synthesized by the present methods showed specific surface area as high as 820 m<sup>2</sup> g<sup>-1</sup>. Therefore, improved ionic conductivity accompanying higher electrolyte swelling of the polypyrrole can explain the slightly higher utilization of sulfur for the cell with a higher amount of electrolyte (7.0 ml/g-S) compared with the cell with lower electrolyte content (5.0 ml/g-S). In addition, a comparison between the cyclability performance of a cell with SPPyMnO<sub>2</sub> electrode and the pristine S-MnO<sub>2</sub> electrode from reference [41], in **Figure S7**, shows a

significant improvement in the performance of the multilayer encapsulated sulfur electrode from our work which verifies the stabilization provided by both the polypyrrole conductive polymer and the inner  $\text{MnO}_2$  shell.

The coulombic efficiency of the cell with SPPy $\text{MnO}_2$  electrode remained above 95% throughout the cycling, which suggests substantial suppression of polysulfide shuttling resulting from the multilayer encapsulation. The specific capacity of the SPPy and bare sulfur electrodes decreased rapidly on cycling by reaching  $936 \text{ mAh g}^{-1}$  and  $238 \text{ mAh g}^{-1}$  after 75 cycles at C/5, respectively while despite the higher C-rate (0.2C) of the cell with SPPy $\text{MnO}_2$  electrode it retained a specific capacity of  $1054 \text{ mAh g}^{-1}$  after 75 cycles. Overall, both electrodes showed lower coulombic efficiency (70% for bare sulfur, 93% for SPPy) than SPPy $\text{MnO}_2$  (>95%). This capacity retention (>93%) is comparable to (a) single layer core-shell composites electrode that was reported by Nazar's group<sup>[34]</sup>, which require providing a void space to prevent any damage to the protective layer due to the volumetric expansion of sulfur during lithiation; is significantly better than (b) polymer encapsulated sulfur particles<sup>[20,21]</sup> and (c) reported values for the mesoporous carbon hosts.<sup>[3]</sup> Such an improvement can be attributed to the efficient reduction in pore size and enhancement in the mechanical stability of the encapsulating layer. This suggests both porosity and physical confinement provided by the multilayer architecture are necessary to trap high-order soluble polysulfides in the cathode.

Voltage profiles collected at C/5 and C/2 rates in coin cells with sulfur loading of  $1.0 \text{ mg/g-S}$  and electrolyte to sulfur ratio of  $\text{E/S} \sim 5 \text{ ml/g-S}$ , present two plateaus, for the SPPy $\text{MnO}_2$  electrode in **Figure 4b**, corresponding to the two-step process of the Li-S battery. SPPy $\text{MnO}_2$  electrode delivers a specific capacity of  $1367 \text{ mAh g}^{-1}$  at C/5 (charge or discharge of 2 Li in 5 hours), corresponding to 81.7% of the theoretical capacity ( $1672 \text{ mAh g}^{-1}$ ). The bare sulfur electrode on the other hand, only

delivers 47% of the theoretical value. Such high utilization in the nano-composite can be attributed to the higher electrical conductivity of the SPPyMnO<sub>2</sub> electrodes despite the fact that the amount of conductive carbon in this electrode is 30% lower than the bare sulfur electrode. It should be noted that contribution of the MnO<sub>2</sub> layer to the capacity is negligible since it only accounts for 2 wt% of the SPPyMnO<sub>2</sub> nano-particles, according to TGA analysis, as shown in **Figure 3**. The voltage window for all cells were adjusted to 1.7-3.0V, to fully allow the cell to discharge.

#### 4. Electrochemical performance of binder-free, high sulfur content SPPyMnO<sub>2</sub>

Study of the techno-economic modeling<sup>[31]</sup> of Li-S batteries suggests that sulfur loading of the electrode is an important factor to achieve sulfur batteries for application in electric highway vehicles. Therefore, we studied multiple electrodes with sulfur loadings as high as 2.7 mg-S cm<sup>-2</sup>. To increase the surface area and to improve the electronic conductivity of the cell, binder-free electrodes have been fabricated by mixing SPPyMnO<sub>2</sub> nano-composite with carbon (super P) in an organic diluent to form a nano-sulfur slurry followed by casting on a P50 carbon paper. Using this technique, uniform electrodes with sulfur loading of 2.5 mg-S cm<sup>-2</sup> and higher were formed. We noticed that presence of the PVDF-binder would increase the resistivity in the electrode, which caused high polarization in the cell and subsequently led to the cell a failure after only few cycles. Cathodes prepared with this method also exhibited typical discharge and charge plateaus for sulfur electrodes when tested in coin cells. We first carried out cycling on a cell with electrode sulfur loading of 2.5 mg-S cm<sup>-2</sup> at C/5 for 20 cycles with subsequent cycling at 1C for 135 cycles. During charging at a current rate of 1C (applied current of 1.225 mA; cathode area of 0.49 cm<sup>2</sup>),

This article is protected by copyright. All rights reserved.

approximately 8  $\mu\text{m}$  of Li metal (30  $\mu\text{mol}$ ) deposits on the lithium foil (assuming uniform and dense plating), which causes the cell to internally short after 135 cycles. Therefore, while the cathode performs well at such C-rate, apparently the anode cannot tolerate such large amount of lithium plating. Similarly, the cell with sulfur loading of 2.7  $\text{mg-S cm}^{-2}$  shorted after 82 cycles at  $\sim 1\text{C}$ .

Despite the high sulfur loading, specific capacity of these cells ( $\sim 1350 \text{ mAh g}^{-1}$ ) were only slightly lower than the cells with lower sulfur loadings (1367  $\text{mAh g}^{-1}$ ) at the same rate of C/5. Surprisingly, the coulombic efficiency for high sulfur loading electrodes was slightly better (approximately 98%) than the lower sulfur containing electrodes (95% efficiency), which can be attributed to the absence of the insulating binder in the high sulfur loading electrodes (**Figure 5a**). In **Figure 5b**, cell voltage versus cycle number for a cell with 2.7  $\text{mg-S cm}^{-2}$  of sulfur and applied current density of 4.5  $\text{mA cm}^{-2}$  demonstrated a voltage loss from 2.45V to 0.2V after 102 cycles during charging when the cell was internally shorted.

##### 5. Self-discharge of the SPPyMnO<sub>2</sub> electrode versus bare-sulfur electrode:

Self-discharge behavior is one of the major challenges for Li-S battery commercialization which has been reported repeatedly.<sup>[32, 54-56]</sup> The capacity decay due to self-discharge in the Li-S battery turned out to be a dramatic issue compared to typical lithium ion batteries, since the capacity can decrease about 50% of its initial value, after 24 hours of storage at room temperature.<sup>[37]</sup>

The self-discharge analysis of our multilayer encapsulated sulfur nanocomposite (SPPyMnO<sub>2</sub>) compared with the bare-sulfur nano-powder electrode exhibited a significant reduction in the capacity decay after 168 hours of rest, as is presented in **figure 6**. This can be attributed to the

This article is protected by copyright. All rights reserved.

successful entrapment of polysulfides within the multilayer encapsulating membrane, which reduces unwanted reactions between long chain polysulfides and the lithium anode. **Figure 6** shows the variation of discharge capacities before and after 168 hours of storage at room temperature. The discharge capacity of the Li-S battery with the bare sulfur electrode is decreased by 34% after 168 hours, while the battery with SppyMnO<sub>2</sub> electrode showed only 9% decay in its capacity. Sulfur loadings in both electrodes were 1.0 mg-S cm<sup>-2</sup> and the coulombic efficiencies for both cells were approximately 95%. The discharge capacities in both electrodes were partially recovered after the first discharge following the rest, which suggests that the self-discharge issue is more likely as a result of the reversible polysulfide shuttling rather than from irreversible loss of the active material.<sup>[57]</sup>

## 6. Conclusion

We demonstrate that through multilayer encapsulation of sulfur particles the polysulfide shuttle can be reduced significantly resulting in a more stable Li-S battery. Sulfur nano-particles are encapsulated with manganese oxide particles as the inner layer and a layer of an electronically conductive polymer as the outer layer. The advantage is that the sulfur particles are surrounded by the encapsulating oxide layer which provides an effective barrier to soluble polysulfides. The polymer coating is added as the outer layer to support the oxide layer and to improve the electronic conductivity of the electrode. This strategy allows stable Li-S cells with high sulfur loading and electrolyte/sulfur ratio as low as 5ml per grams of sulfur. We show that addition of the oxide layer significantly improves the cyclability of the Li-S battery. Compared with the non-encapsulated sulfur

electrode, our multilayer encapsulated sulfur electrode demonstrates improved coulombic efficiency and nominal self-discharge. We also demonstrated that our multilayer encapsulated binder-free electrode shows a somewhat improved coulombic efficiency (98%) over an electrode with 10% binder (95%). Ease of the fabrication, effectiveness and scalability are benefits of this methodology.

## 7. Experimental Section

*Synthesis:* Sulfur nanoparticles were prepared by reacting concentrated hydrochloric acid (1.0 ml, 36-37% wt%, BDH Aristar@ Plus) with aqueous solution of sodium thiosulfate (150 ml, 42.16 mM, 99%, Sigma-Aldrich) containing polyvinylpyrrolidone (PVP, 0.5 wt%,  $M_w \sim 40,000$ , Sigma-Aldrich) for 1 hour. Then, sulfur nanoparticles (150ml) were washed by centrifugation and dispersed into an aqueous solution of PVP (60 ml, 1 wt%) to form a sulfur suspension.

To prepare the SPPy nano-composite, sulfur suspension (60 ml) was added to aqueous solution (80 ml) of iron (III) chloride (0.46 g, 35.45 mM, Sigma-Aldrich), methyl orange (10mg, 0.38 mM, Fluka) and PVP (0.75 wt%). Aqueous solution of pyrrole (20 ml, 150 mM, Sigma-Aldrich) was then added dropwise in 20 minutes. After reacting for 3 hours, SPPy was collected by centrifugation and was washed three times with deionized water (160 ml) and dilute hydrochloric acid solution (160 ml, 0.25 M), alternatively. Afterwards, the brown centrifuged nano-powder was dispersed in aqueous solution of ammonium persulfate (100ml, 43.8 mM, Sigma-Aldrich) and stirred for 45 minutes at room temperature. Then, the light-brown nano-powder was washed three times with deionized water (160ml). SPPy nano-composite powder was then dried in a gravity convection oven at 60°C for 24 hours or reacted with  $KMnO_4$  to form SPPy $MnO_2$  nano-particles.

This article is protected by copyright. All rights reserved.

To form SPPyMnO<sub>2</sub> nano-particles, SPPy nano-composite was dispersed into deionized water (40 ml). Aqueous solution of KMnO<sub>4</sub> (80 ml, 2.5 mM, Sigma-Aldrich) was dropwise added to the SPPy suspension and was let to react under continuous stirring at room-temperature. After reacting for 3 hours, the solution of SPPyMnO<sub>2</sub> nano-composite was washed twice with deionized water (100 ml) followed by vacuum drying.

*Electrochemical measurements:* Low sulfur content working electrodes were prepared by mixing the nano-powder with carbon black and PVDF binder by weight percentages of 70:20:10 in NMP to form a slurry. The slurry was then tape-casted onto an aluminum foil using a doctor blade and was initially dried at 50°C for 24 hours, followed by vacuum drying, overnight. Bare sulfur slurry was prepared by mixing sulfur nano-particles with carbon black and PVDF (50:40:10 by weight) in NMP. All cells were rested at room-temperature for 6 hours prior to the test.

High sulfur content working electrodes were fabricated by mixing the nano-powder with carbon black by weight percentages of 80:20 in DOL/DME (50:50) to form a slurry. The slurry was then drop-casted on P50 carbon followed by drying at 50°C for 24 hours under argon atmosphere.

Half-cells were assembled into coin cells under argon atmosphere using lithium metal foil as the counter electrode. A solution of lithium bis(trifluoromethanesulfonyl)imide (TFSI) (1 M) in 1,3-dioxolane and 1,2-dimethoxyethane (DOL/DME, 1:1 v/v) containing lithium nitrate (1 wt%) was used as the electrolyte. A 16 channel BioLogic VMP3 multi-potentiostat/galvanostat was used to carry out galvanostatic cycling of the cells from 1.7-3.0 V versus Li/Li<sup>+</sup>.

*Characterizations:* Transmission Electron Microscopy (TEM) images were taken using a FEI Tecnai (G2 Spirit TWIN) with an accelerating voltage of 40kV, and the Scanning Electron Microscopy (SEM)

images were taken using a Zeiss Merlin High-resolution instrument with an accelerating voltage of 5kV. Elemental analysis was performed using energy-dispersive X-ray spectroscopy equipped to the SEM and TEM instruments. Thermogravimetric analysis was carried out using a SDT Q600 Simultaneous TGA/DSC instrument. The results of elemental analysis and thermogravimetric analysis were used to calculate specific capacity values based on the mass of sulfur in each composite. X-ray diffraction patterns were obtained by a PANalytical X'Pert Diffractometer. Inductively coupled plasma optical emission spectroscopies were performed using an Agilent Technologies 7700 Series ICP-MS spectrometer. Nitrogen adsorption tests were performed on a Micromeritics ASAP 2020 Surface Area and Porosity analyzer.

### Supporting Information

Supporting Information is available from the Wiley Online Library or from the author.

**Acknowledgement:** This work is supported as part of the Joint Center for Energy Storage Research (JCESR), an Energy Innovation Hub funded by the U.S. Department of Energy, Office of Science, Basic Energy Sciences. Electron microscopy and X-ray diffraction was conducted within the MIT Center for Materials Science and Engineering, a MRSEC Shared Experimental Facility supported by the National Science Foundation under award number DMR-14-19807.

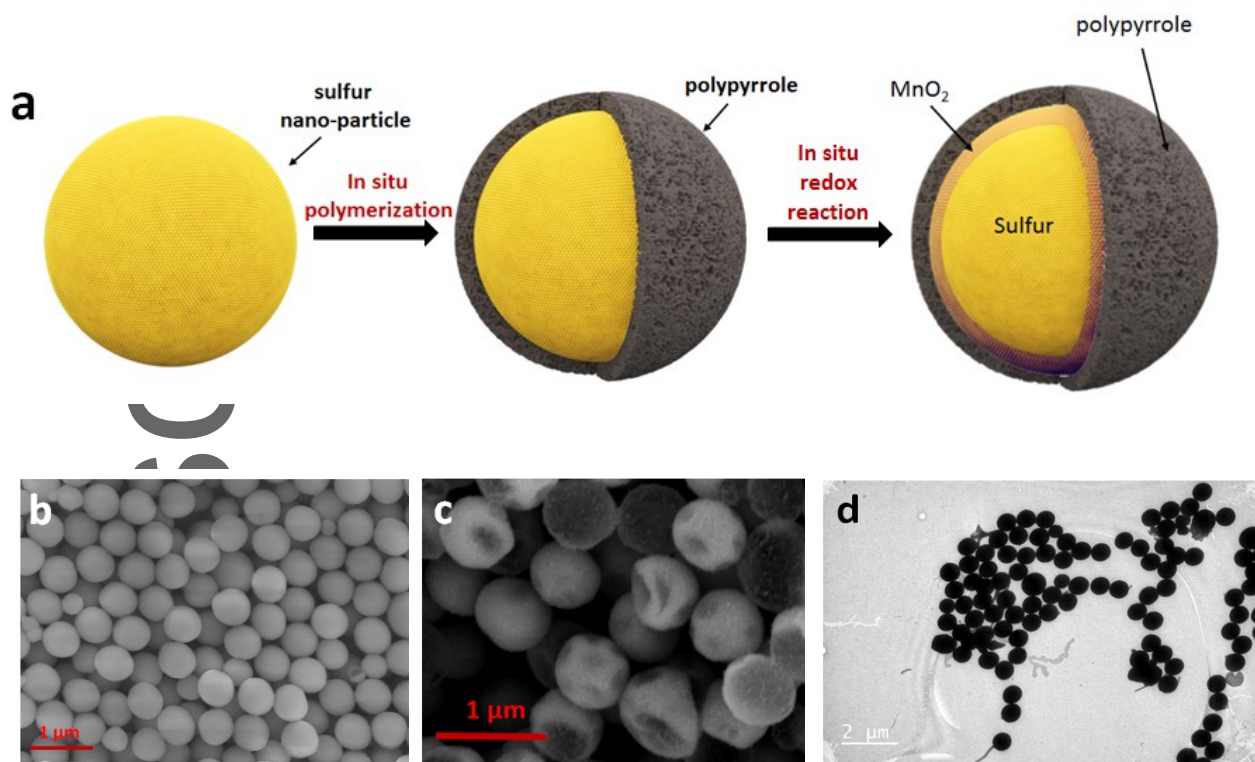


**Figure 1.** (a) Schematic of the process for the synthesis of SPPyMnO<sub>2</sub> nano-composite, (b) SEM image of SPPy, (c) SEM image of the SPPyMnO<sub>2</sub>, and (d) TEM image of the SPPyMnO<sub>2</sub>.

Author Manuscript

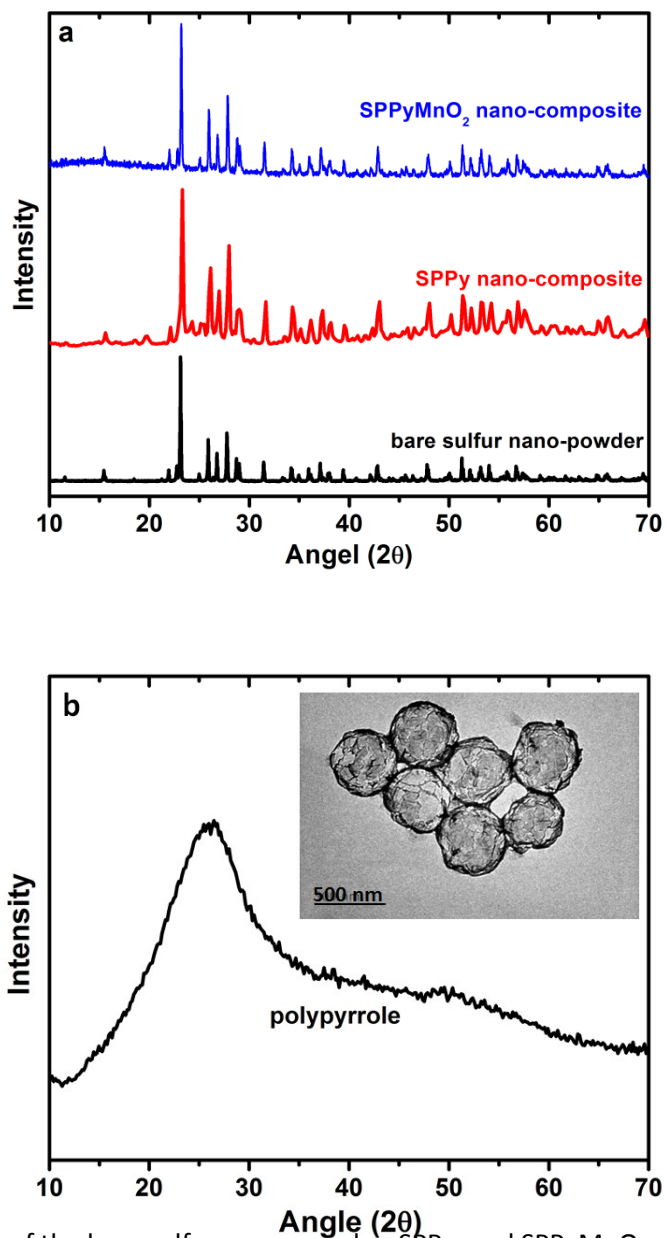


**Figure 2.** (a) XRD pattern of the bare sulfur nano-powder, SPPy, and SPPyMnO<sub>2</sub> nano-composites. (b) XRD pattern of polypyrrole produced through the oxidative polymerization of pyrrole. Inset is the SEM image of the Polyporrole/MnO<sub>2</sub> shell, after the dissolution of sulfur core.

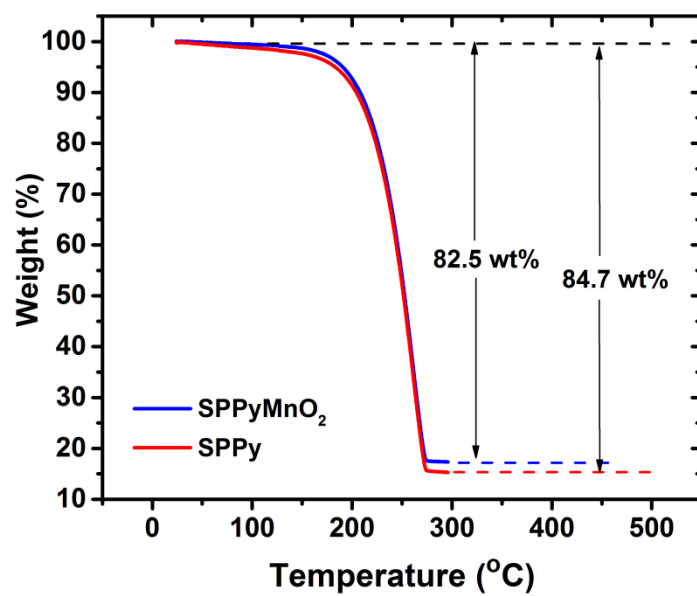


**Figure 3.** TGA curves of the pristine SPPy (red) and SPPyMnO<sub>2</sub> (blue) nano-composites.

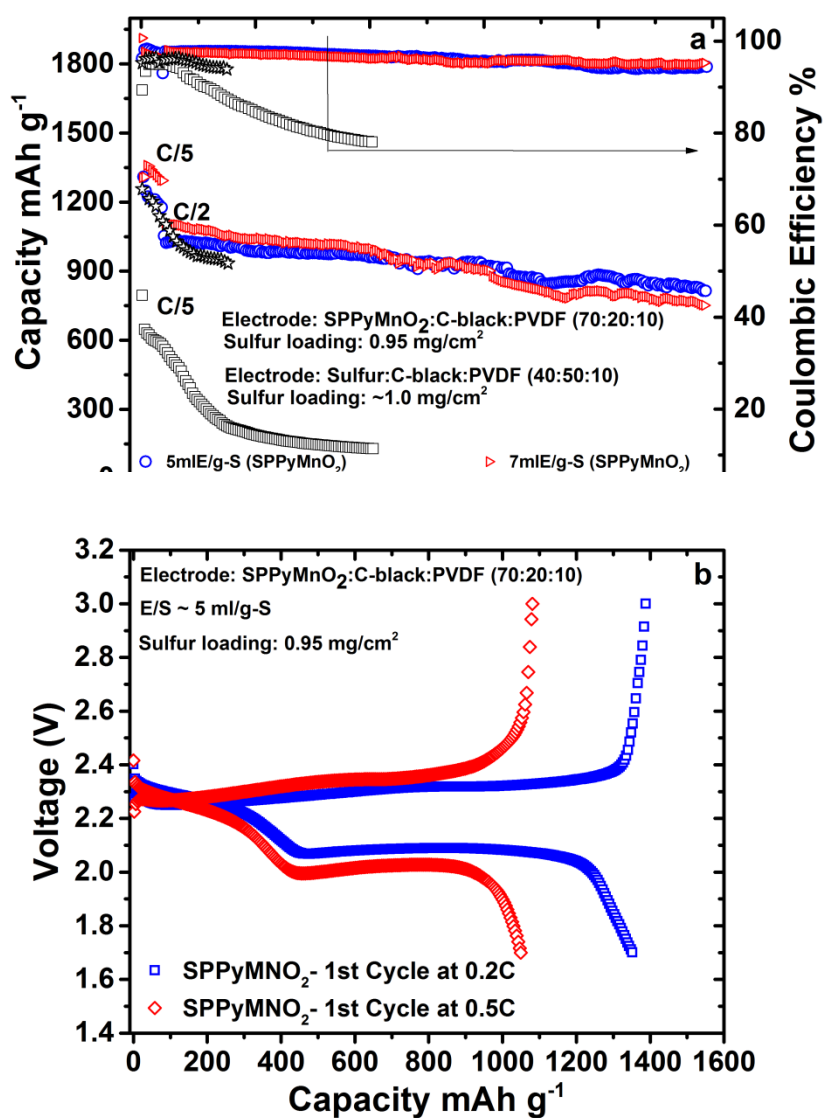


**Figure 4.** (a) Comparison of the efficiency and cycle performance of the bare sulfur, SPPy, and SPPyMnO<sub>2</sub> electrodes. Cyclability of the SPPyMnO<sub>2</sub> electrodes with 7 ml/g-S and 5 ml/g-S are also compared. (b) Voltage profile for the first cycle of the SPPyMnO<sub>2</sub> electrodes at C/5 and C/2. Sulfur loading of tested electrodes are 0.95 mg cm<sup>-2</sup>.

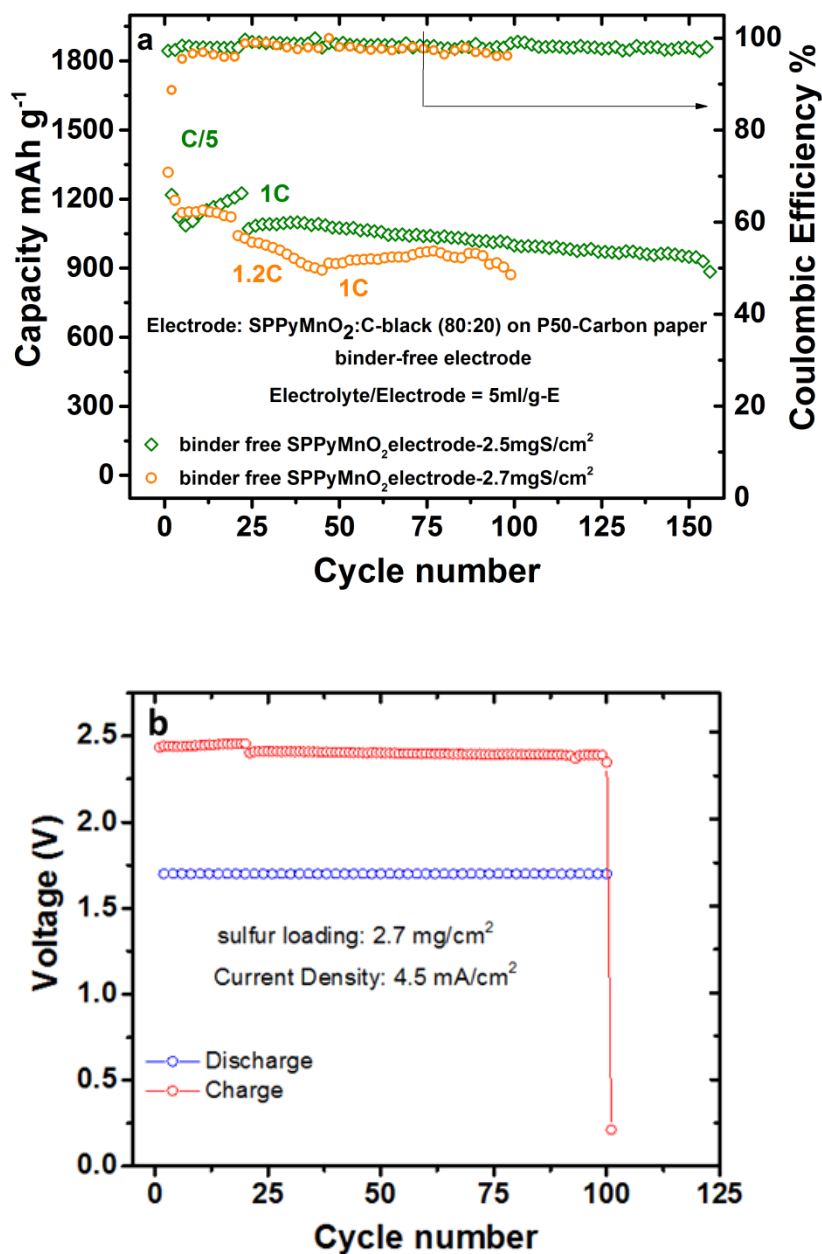


**Figure 5.** (a) Comparison of the efficiency and cycle performance of SPPyMnO<sub>2</sub> electrodes with 2.5 mg-S cm<sup>-2</sup> and 2.7 mg-S cm<sup>-2</sup> at C/5 and 1C. (b) Corresponding plot of voltage versus cycle number for the cell with 2.7 mg-S cm<sup>-2</sup> showing the sudden drop in the voltage after 100 cycles of discharge and charge with a max current density of 4.5 mA cm<sup>-2</sup> due to the short-circuit.

This article is protected by copyright. All rights reserved.

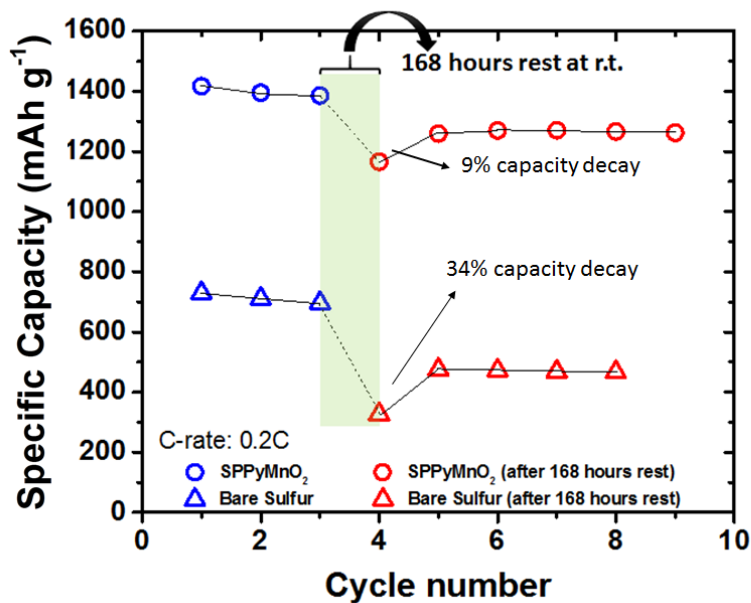
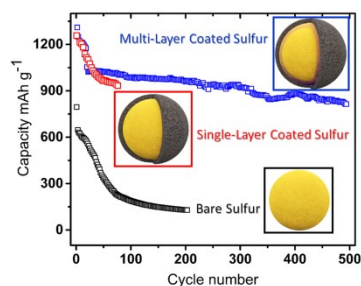


**Figure 6.** Comparison of changes in the discharge capacity of bare sulfur and SPPyMnO<sub>2</sub> electrodes with identical amount of sulfur at C/5 before (blue) and after (red) 168 hours of rest at room-temperature.

A stable lithium sulfur battery is enabled by a multi-layer encapsulated sulfur nanocomposite electrode. The inner coating layer is a metal-oxide capable of anchoring long-chain polysulfides and the outer coating layer is a conductive porous polymer resulting in a battery with more than 500 cycles.

>>>> 299 characters with spaces



This article is protected by copyright. All rights reserved.

## References

- 
- [1] W. Freyland, A. Goltzene, P. Grosse, G. Harbeke, H. Lehmann, O. Madelung, W. Richter, C. Schwab, G. Weiser, H. Werheit, W. Zdanowicz, Landolt-Börnstein, Numerical Data and Functional Relationships in Science and Technology. Vol. 17 (Ed: O. Madelung) Springer-Verlag Berlin, Heidelberg, Germany **1983**, p.78.
- [2] J. L. Wang, J. Yang, J. Y. Xie, N. X. Xu, *Adv. Mater.* **2002**, 14, 963.
- [3] C. D. Liang, N. J. Dudney, J. Y. Howe, *Chem. Mater.* **2009**, 21, 4724.
- [4] X. Ji, K. T. Lee, L. F. Nazar, *Nat. Mater.* **2009**, 8, 500.
- [5] Y. Yang, M. T. McDowell, A. Jackson, J. Cha, S. S. Hong, Y. Cui, *Nano Lett.* **2010**, 10, 1486.
- [6] Y. Yang, G. Yu, J. J. Cha, H. Wu, M. Vosgueritchian, Y. Yao, Z. Bao, Y. Cui, *ACS Nano* **2011**, 5, 9187.
- [7] L. Yin, J. Wang, J. Yang, Y. Nuli, *J. Mater. Chem.* **2011**, 21, 6807.
- [8] R. Elazari, G. Salitra, A. Garsuch, A. Panchenko, D. Aurbach, *Adv. Mater.* **2011**, 23, 5641.
- [9] X. Ji, S. Evers, R. Black, L. F. Nazar, *Nat. Commun.* **2011**, 2, 325.
- [10] G. Zheng, Y. Yang, J. J. Cha, S. S. Hong, Y. Cui, *Nano Lett.* **2011**, 11, 4462.
- [11] J. Guo, Y. Xu, C. Wang, *Nano Lett.* **2011**, 11, 4288.
- [12] N. Jayaprakash, J. Shen, S. S. Moganty, A. Corona, L. A. Archer, *Angew. Chem. Int. Ed.* **2011**, 50, 5904.

- [13] H. Wang, Y. Yang, Y. Liang, J. T. Robinson, Y. Li, J. Jackson, Y. Cui, H. Dai, *Nano Lett.* **2011**, *11*, 2644.
- [14] L. Ji, M. Rao, H. Zheng, L. Zhang, Y. Li., W. Duan, J. Guo, E. J. Cairns, *J. Am. Chem. Soc.* **2011**, *133*, 18522.
- [15] F. Wu, J. Chen, R. Chen, S. Wu, L. Li, S. Chen, T. Zhao, *J. Phys. Chem. C* **2011**, *115*, 6057.
- [16] X. Liang, Y. Liu, Z. Wen, L. Huang, X. Wang, H. Zhang, *J. Power Sources* **2011**, *196*, 6951.
- [17] L. Su, Y. Jing, Z. Zhou, *Nanoscale* **2011**, *3*, 3967.
- [18] J. Schuster, H. He, B. Mandlmeier, T. Yim, K. T. Lee, T. Bein, L. F. Nazar, *Angew. Chem. Int. Ed.* **2012**, *51*, 3591.
- [19] L. Xiao, Y. Cao, J. Xiao, B. Schwenzer, M. H. Engelhard, L. V. Saraf, Z. Nie, G. J. Exarhos, J. Liu, *Adv. Mater.* **2012**, *24*, 1176.
- [20] Y. Fu, A. Manthiram, *RSC Adv.* **2012**, *2*, 5927.
- [21] Y. Fu, A. Manthiram, *J. Phys. Chem. C* **2012**, *116*, 8910.
- [22] Y. Fu, A. Manthiram, *Chem Mater.* **2012**, *24*, 3081.
- [23] X. Li, P. Meduri, X. Chen, W. Qi, M. H. Engelhard, W. Xu, F. Ding, J. Xiao, W. Wang, C. Wang, J. -G. Zhang, J. Liu, *J. Mater. Chem.* **2012**, *22*, 11014.
- [24] X. Liang, Z. Wen, Y. Liu, H. Zhang, J. Jin, M. Wu, X. Wu, *J. Power Sources* **2012**, *206*, 409.
- [25] L. Wang, D. Wang, F. Zhang, J. Jin, *Nano Lett.* **2013**, *13*, 4206.
- [26] Z. W. Seh, W. Li, J. J. Cha, G. Zheng, Y. Yang, M. T. McDowell, P. -C. Hsu, Y. Cui, *Nat. Commun* **2013**, *4*, 1331.
- [27] Z. Dong, J. Zhang, X. Zhao, J. Tu, Q. Su, G. Du, *RSC Adv.* **2013**, *3*, 24914.
- [28] G. Yuan, H. Wang, *J. Energy Chem.* **2014**, *23*, 657.

- [29] X. Liang, C. Hart, Q. Pang, A. Garsuch, T. Weiss, L. F. Nazar, *Nat. Commun* **2015**, 6, 5682.
- [30] S. Chen, X. Huang, H. Liu, B. Sun, W. Yeoh, K. Li, J. Zhang, G. Wang, *Adv. Energy Mater.* **2014**, 4, 1301761.
- [31] W. Bao, D. Su, W. Zhang, X. Guo, G. Wang, *Adv. Funct. Mater.* **2016**, 26, 8746.
- [32] D. Su, M. Cortie, G. Wang, *Adv. Energy Mater.* **2017**, 7, 1602014.
- [33] Y. Chen, S. Choi, D. Su, X. Gao, G. Wang, *Nano Energy* **2018**, 47, 331.
- [34] J. Xu, W. Zhang, Y. Chen, H. Fan, D. Su, G. Wang, *J. Mater. Chem. A* **2018**, 6, 2797.
- [35] D. Su, M. Cortie, H. Fan, G. Wang, *Adv. Mater.* **2017**, 29, 1700587.
- [36] W. Bao, L. Liu, C. Wang, S. Choi, D. Wang, G. Wang, *Adv. Energy Mater.* **2018**, 8, 1702485.
- [37] J. Wang, J. Chen, K. Konstantinov, L. Zhao, S.H. Ng, G.X. Wang, Z.P. Guo, H.K. Liu, *Electrochimica Acta* **2006**, 51, 4634.
- [38] H. S. Ryu, H. J. Ahn, K. W. Kim, J. H. Ahn, K. K. Cho, T. H. Nam, *Electrochimica Acta* **2006**, 52, 1563.
- [39] J. Zheng, D. Lv, M. Gu, C. Wang, J. -G. Zhang, J. Liu, J. Xiao, *J. Electrochem. Soc.* **2013**, 160, A2288.
- [40] D. Eroglu, K. R. Zavadil, K. G. Gallagher, *J. Electrochem. Soc.* **2015**, 162, A982.
- [41] X. Liang, and L. F. Nazar, *ACS Nano* **2016**, 10, 4192.
- [42] H. Mi, X. Zhang, Y. Xu, F. Xiao, *Appl. Surf. Sci.* **2010**, 256, 2284.
- [43] X. Yang, Z. Zhu, T. Dai, Y. Lu, *Macromol. Rapid Commun.* **2005**, 26, 1736.
- [44] H. J. Kharat, K. P. Kakade, P. A. Savale, K. Dutta, P. Ghosh, M. D. Shirsat, *Polym. Adv. Technol.* **2007**, 18, 39.

- [45] K. Arora, A. Chaubey, R. Singhal, R. P. Singh, M. K. Pandey, S. B. Samanta., B. D. Malhotra, S. Chand, *Biosens. Bioelectron.* **2006**, 21, 1777.
- [46] B. Tian, G. Zerbi, *J. Phys. Chem.* **2009**, 92, 3886.
- [47] M. A. Chougule, S. G. Pawar, P. R. Godse, R. N. Mulik, S. Sen, V. B. Patil, *Soft Nanoscience Letters*, **2011**, 1, 6.
- [48] R. Steudel, Topics in Current Chemistry: Elemental Sulfur and Sulfur-Rich Compounds II. Vol. 231, Springer-Verlag Berlin Heidelberg, Germany **2003**, p.54-55.
- [49] H. W. Nesbitt, D. Banerjee, *American Mineralogist* **1998**, 83, 305.
- [50] J. Shen, A. Liu, Y. Tu, *Electrochimica Acta.* **2012**, 78, 122.
- [51] A. Aygun, J. W. Buthker, L. D. Stephenson, A. Kumar, T. K. Mahle, A. A. Gewirth, *J. Electroanal. Chem.* **2012**, 684, 47.
- [52] S. D. O. Costa, J. J. L. Cascales, *J. Electroanal. Chem.* **2010**, 644, 13.
- [53] G. L. Duffitt, P. G. Pickup, *J. Chem. Soc. Faraday Trans.* **1992**, 88, 1417.
- [54] Y. V. Mikhaylik, J.R. Akridge, *J. Electrochem. Soc.* **2004**, 151, A1969.
- [55] H. S. Ryu, H. J. Ahn, K. W. Kim, J. H. Ahn, J. Y. Lee, E. J. Cairns, *J. Power Sources* **2005**, 140, 365.
- [56] H. S. Ryu, H. J. Ahn, *Mater. Sci. Forum* **2005**, 486, 630.
- [57] L. Wang, J. Liu, S. Yuan, Y. Wang and Y. Xia, *Energy Environ. Sci.* **2016**, 9, 224.